Development of a copper-graphene nanocomposite based transparent coating with antiviral activity against influenza virus

Indrani Das Jana[1#], Partha Kumbhakar[2#], Saptarshi Banerjee[1], Chinmayee Chowde Gowda[3], Nandita Kedia[1], Saikat Kumar Kuila[2], Sushanta Banerjee[4], Narayan Chandra Das[5], Amit Kumar Das[1], Indranil Manna[2], Chandra Sekhar Tiwary[2*], Arindam Mondal[1*]

[1]School of Bioscience, Indian Institute of Technology Kharagpur, India

[2]Department of Metallurgical and Materials Engineering, Indian Institute of Technology Kharagpur, India

[3]School of Nanoscience and Technology, Indian Institute of Technology Kharagpur, India

[4]Material Science Center, Indian Institute of Technology Kharagpur, India

[5]Rubber Technology Center, Indian Institute of Technology Kharagpur, India

# Authors contributed equally

* Address for correspondence: arindam.mondal@iitkgp.ac.in, chandra.tiwary@metal.iitkgp.ac.in

Keywords: Nanocomposite, Influenza virus, Nano-Luciferase, Antivirals coating

Abstract

Respiratory infections by RNA viruses are one of the major burdens upon global health and economy. Viruses like influenza or coronaviruses can be transmitted through respiratory droplets or contaminated surfaces. An effective antiviral coating can decrease the viability of the virus particles in the outside environment significantly, hence reducing their transmission rate. In this work, we have screened a series of nanoparticles and their composites for antiviral activity using Nano Luciferase based highly sensitive influenza A reporter virus. Using this screening system, we have identified copper-graphene (Cu-Gr) nanocomposite shows strong antiviral activity. Extensive material and biological characterization of the nanocomposite suggested a unique metal oxide embedded graphene sheet architecture that can inactivate the virion particles only within 30 minutes of pre-incubation and subsequently interferes with the entry of these virion particles into the host cell. This ultimately results in reduced viral gene expression, replication and production of progeny virus particles, slowing down the overall pace of progression of infection. Using PVA as a capping agent, we have been able to generate a Cu-Gr nanocomposite based highly transparent coating that retains its original antiviral activity in the solid form.

Introduction

The emergence of novel virus strains and the associated outbreaks are becoming a significant threat to mankind (Koven 2020). The currently ongoing pandemic, caused by the Severe Acute Respiratory Syndrome- Coronavirus 2 (SARS-CoV-2), has brought the majority of the world to a grinding halt, severely impacting health & economy across the nations (Letko, Marzi, and Munster 2020). So far, the COVID-19 pandemic has claimed 720,000 lives resulting from 19.4 million infections globally. This reminds us of the great 1918 Spanish flu pandemic by the influenza virus, which resulted in 500 million infections with 50 million deaths (Johnson and Mueller 2002) (Patterson and Pyle 2019) (Taubenberger and Morens 2006) (Landrigan et al. 2018). Till date, there have been four worldwide pandemics caused by influenza viruses in the last century (1918, 1957, 1968, 2009) (World Health Organization 2018) (Saunders-Hastings and Krewski 2016), while Covid19 is the first pandemic caused by the Coronavirus (Y. Wu et al. 2020). Other than pandemics, influenza A and B viruses cause seasonal outbreaks (290,000 to 650,000 deaths worldwide: CDC FLUVIEW] and different coronaviruses cause mild flu-like symptoms to severe respiratory infections (SARS (De Wit et al. 2016) and MERS (Lin et al. 2019) coronavirus epidemics during 2002 and 2012 respectively) (Fehr and Perlman 2015). Clearly, recurring respiratory infections caused by these viruses are becoming one of the global human health problem.

Both influenza and coronaviruses cause respiratory infections, which can be transmitted from infected to healthy individuals through respiratory droplets, aerosols or contacts. These respiratory pathogens are known for their ability to persist on inanimate surfaces for days and even up to months, depending upon weather conditions (Vasickova et al. 2010). As a result, touching contaminated surfaces in public places is a potential route of viral transmission. In fact, the inanimate surfaces have been identified as a major cause of infections, especially in institutions where individuals are in contact with patients or contaminated fomites. Thus, the development of low cost and easily scalable antiviral coating materials, which could be widely applied to various surfaces in order to inactivate the virus particles in the environment, may serve as an effective way to reduce the chance of infection and hence to lower the overall speed of transmission.

Different metal oxides, including Cu and Ag have been explored for their biocidal activity in soluble as well as in insoluble forms (Minoshima et al. 2016) . Copper and silver nanoparticles have remarkable properties like high electrical and thermal conductivity (Barani et al. 2020; D. Deng et al. 2013), superior catalytic nature (Gawande et al. 2016), anti-fungal (Cioffi et al. 2005) and bacteriostatic activities (Ruparelia et al. 2008) to name a few. Solid-state cuprous oxide and silver nitrate have been shown to inactivate virus particles through interfering with the activity of the surface antigen, hemagglutinin (HA), thereby blocking

the attachment of the virus to the host cell receptors (Fehr and Perlman 2015) (Sunada, Minoshima, and Hashimoto 2012). Cuprous oxide nanoparticles had also been shown to inhibit the attachment and entry stages of Hepatitis C Virus infection, hence suggesting a generic mechanism for the copper-based nanoparticles for their antiviral activities (Hang et al. 2015). This may also explain the lesser viability of infectious SARS-CoV-2 particles on copper surfaces (8 h) when compared to stainless steel and plastic surfaces (72 h) (Neeltje van Doremalen et al. 2020). Biological activity of the Cu or Ag nanoparticles largely depends upon their size, shape, stability and capping agent. Due to the high reactivity of these nanoparticles, they can undergo rapid agglomeration leading to the drastic reduction of their activity (Ma et al. 2011). One way to overcome this instability is to form a composite with other organic or inorganic compounds which stabilizes the nanoparticles by altering their surface architecture (Perdikaki et al. 2018).

Graphene is composed of a single atom thick sheet of sp2 hybridized carbon atoms that forms a honeycomb lattice (Mohammed et al. 2020; Palmieri and Papi 2020). This structure of graphene is responsible for its large surface area, excellent electrical conductivity, strong mechanical strength and unique physicochemical properties (Edwards and Coleman 2013; Eigler and Hirsch 2014; Novoselov et al. 2012). It is used extensively in the field of nano-medicine due to easy surface functionality and controlled selectivity (Park et al. 2020). In recent times, the two dimensional sheet of graphene has caught much attention due to its antimicrobial and antiviral activity (Georgakilas et al. 2012). Differentially functionalized graphene oxide sheets can warp and encapsulate microorganisms, thereby severely restricting their interaction with host cells (Perdikaki et al. 2018) (Vinothini and Rajan 2017) (Karahan et al. 2018). For example, sulfate functionalized reduced graphene oxide has been shown to interact with the positively charged surface proteins of different orthopoxvirus strains (Ziem et al. 2016) (Ye et al. 2015). In this work, we have performed an extensive investigation of the potential antiviral activity of copper (Cu) nanoparticles, silver (Ag) nanoparticles, graphene (Gr) and their hybrid versions (nanocomposite materials) Ag-graphene, Cu-graphene and Ag-Cu-graphene against respiratory viruses using influenza A virus as a model system. Our data shows that prior incubation with the colloidal Cu-Gr nanocomposite can impose a strong reduction in viral infectivity, which gets manifested in the reduced viral entry, gene expression and subsequent production of progeny virions. Extensive material characterization using UV-Visible absorption and Raman spectroscopy along with X-Ray Diffraction (XRD) reveals a unique architecture of copper oxide decorated two-dimensional graphene sheets. The shape, size and distribution of the hybrid nanoparticles were also studied using Scanning Electron Microscopy (SEM) and Energy-dispersive X-ray spectroscopy (EDAX). Finally, we have developed for the first time a polyvinyl alcohol (PVA) based copper-graphene nanocomposite coating, which is completely transparent and shows strong antiviral activity in the solid phase.

Results

Synthesis and preliminary characterization of the nanoparticles and nanocomposites

We have synthesized various nanoparticles and their hybrids using a simple and cost-effective chemical method as discussed in the experimental section. The synthesized materials are Cu nanoparticles, Ag nanoparticles, graphene (Gr) and their hybrid versions Ag- graphene, Cu- graphene and Ag-Cu-graphene (Figure 1 A, B). Visible absorption spectra of each of these variants confirms the presence of respective components either alone or in combination with their composite partners, as shown in Figure 1C and D. The peak at 418 nm confirms the formation of Ag colloidal nanoparticles (Jin et al. 2005). From literature, it is attributed to Surface Plasmon Resonance with spherical nature (Hu et al. 2013). From the UV-vis spectra of the composite Ag-Gr, Plasmon absorption band at around 410 nm, indicates the formation of a hybrid structure. Incorporation of Ag nanoparticles on graphene sheets had led to a blue shift of the surface plasmon resonance, a characteristic similar to previous reports (Kim et al. 2018).

Furthermore, Cu nanoparticles, due to exposure of air at room temperature, goes through surface oxidation, which is the reason that samples contain oxygen in +1 and +2 states forming CuO or Cu_2O (Yao et al. 2005). Composite including both Ag and Cu nanoparticles were also analyzed from the absorption spectrum. A broad graphene peak was observed at 280 nm in the composite. Both Ag and Cu nanoparticle plasmon peaks were observed and confirmed the presence of the colloidal nanoparticles on graphene sheets (Darabdhara et al. 2017). Particularly, Figure 1D shows the absorption spectra of the composites and it confirms the formation of graphene and CuO/Cu_2O nanoparticles. An absorption peak at 262 nm is due to $\pi \rightarrow \pi^*$ transition in C=C bond of graphene. Another absorption band at~350-450 nm is attributed to the intrinsic band to band transition of the CuO and Cu_2O (Zhang et al. 2020). A blue shift was observed in the peak position compared to bulk CuO; this might be due to the quantum confinement effects exhibited by the particle when the size varies from bulk to nano. These UV-Vis peaks were well matched with CuO and Cu_2O absorption profiles from previous studies (Chan et al. 2007). A broadened plasmon resonance peak for Cu-Gr nanocomposites is due to irregular shapes and sizes of the particles (Zhang et al. 2020).

Screening of nanoparticles and their hybrids for antiviral activity

To test the antiviral activity of synthesized nanomaterials and their composites we have used a bioluminescent reporter variant of the influenza A virus, strain A/H1N1/WSN/1933, that has been previously reported by Tran et al. (Tran et al. 2013). This virus has a Nano-Luciferase (NLuc) gene fused to the carboxy-terminal of the viral PA gene, interspaced by the “self-cleaving” 2A peptide encoding

sequence from porcine teschovirus. The Nano-Luc-influenza A reporter virus, as a part of its gene expression, synthesizes the PA-2A-NLuc polypeptide, which gets self-cleaved to produce Nano-luciferase. Subsequently, the luciferase activity could be measured as a quantitative estimate of viral gene expression and hence progression of virus replication cycle inside the cells. To test whether the Nano-luciferase activity could actually serve as a proxy to virus replication, we have infected MDCK cells with different amounts of input virus and viral replication/gene expression was monitored using Nano-Glo assay (Promega). As shown in Figure 3A, there is a linear relationship between multiplicity of infection (0.01-0.1) and luciferase light unit measurements (R^2= 0.9294), where an increase in one log in the input virus amount leads to about 50% increase in the luciferase activity or vice versa, measured at 8 hours of post-infection. This data suggests that the Nano-luciferase influenza A reporter virus could serve as an excellent tool to study the antiviral activity of various nanoparticles or their nanocomposites used in this study.

In order to test the antiviral activity, we have standardized a "Nano-Luc reporter assay" described in Figure 3B. Briefly, Nano-luciferase influenza A reporter viruses were pre-incubated with the 5uM colloidal suspensions of each of the nanoparticles/ composites or with the vehicle control for 30 minutes at room temperature and subsequently used to infect MDCK cells at an MOI of 0.1. Luciferase activity was measured at 8 hours of post infection and plotted as a relative percentage of the vehicle control set (Figure 3C). Prior treatment of the virus stock solution with Cu-Gr composite showed 64% reduction in viral gene expression, while prior treatment with Ag-Gr resulted in 20% reduction. Treatment with other materials shows no significant decrease in luciferase activity. From the correlation of input virus units and the corresponding luciferase activity, as shown in Figure 3A, it can be inferred that prior treatment with Cu-Gr solution resulted in more than 10-fold reductions in the infectious virus population that has been used to infect the MDCK cells. In this context, it should be noted that none of the materials showed substantial cytotoxicity upon Madin-Darby Canine Kidney cells (MDCK) within the concentration range of 0.5 uM - 5.0 uM as evaluated using MTT assay (Figure 2). Hence, the reduction in Nano-luciferase activity as a result of prior exposure to Cu-Gr should be attributed exclusively to the reduction of the infectivity of the Nano-luciferase reporter virus. Henceforth, we focused upon the extensive characterization of the Cu-Gr nanocomposite.

Material characterization of Cu-Gr nanocomposite

We have extensively characterized the structural parameters of the synthesized Cu-Gr nanocomposites by optical measurements. Figure 4 A depicts Raman spectra of synthesized Cu-Gr nanocomposite samples at excitation of 532 nm in the range of 200 cm^{-1} to 3000 cm^{-1}. With Raman spectroscopy, we are able to distinguish both pristine graphene and copper peaks. The presence of D peak (1361 cm^{-1}) and G peak (1527

167 cm^{-1}) confirms the existence of graphene in the samples synthesized. Generally, D peak originates from
168 defects in the hexagonal sp^2 carbon system while the G peak arises due to the stretching vibration of sp^2
169 carbon pairs in both rings and chains (Ferrari et al. 2006). Except, D and G peak, the 2D peak arises at
170 ~2700 cm^{-1}. The 2D peak originates due to transverse optical (TO) phonons around the K point and is
171 activated by triple resonance Raman scattering (TRRS) (J. Bin Wu et al. 2018). In the measured Raman
172 spectra (Figure 4B), three peaks are (280 cm^{-1}, 350 cm^{-1} and 654 cm^{-1}) observed to confirm the formation
173 of oxide of Cu and originate due to the first order phonon scattering. The peaks are assigned to A_g and $2B_g$
174 peaks of copper oxide (Y. Deng et al. 2016). The graphene sheets are also seen in the optical images, as
175 shown in the inset of Figure 4 A. Figure 4B shows the XRD patterns of graphene, CuO, and Cu_2O
176 nanoparticles, which confirm the crystalline phase of composites samples (standard JCPDS file number 35–
177 0505, 80–1917). Interestingly, the intensity of the Cu_2O is more intense compared to that of the CuO peaks,
178 suggesting a higher abundance of Cu_2O on the surface of the graphene sheets. No diffraction peaks
179 corresponding to impurities are observed in the patterns.
180

181 **Extensive characterization of antiviral property of Colloidal Cu-Gr nanocomposite**
182 Followed by the material characterization, we have invested significant efforts for the characterization of
183 the antiviral property of the Cu-Gr nanocomposites in its colloidal form. First, we have used the Nano-Luc
184 reporter assay in order to identify the optimal time and concentration required for its antiviral activity. The
185 Nano-Luc reporter assay was performed where the influenza A reporter virus was pretreated with the
186 colloidal form of the Cu-Gr nanocomposite for various time periods before using them for infecting MDCK
187 cells. As evidenced from Figure 5A, a sharp decrease (>50%) in the reporter activity was observed as a
188 result of 30 minutes of preincubation with Cu-Gr composite, while longer times of preincubation showed
189 only minor additional reduction. This data suggested that 30 minutes of preincubation with Cu-Gr
190 composite can lead to more than tenfold reduction in input virus titer that ultimately results in ~50%
191 decrease in reporter activity. Subsequently, we tried to identify the optimal concentration of the Cu-Gr
192 composite required for its antiviral activity. Different concentrations of the Cu-Gr composite (50nM,
193 100nM, 500nM, 1µM, 2µM and 5µM, respectively) were used to treat the Nano-Luc influenza A reporter
194 virus for 30 minutes followed by performing Nano-Luc reporter assay with the same. A precise dose
195 dependent decrease in reporter activity and hence virus replication was observed as a result of prior
196 treatment with Cu-Gr composite within the concentration range of 0.5mM to 5mM (Figure 5B). While
197 higher concentration (10µM) further reduced reporter activity, it may also show cytotoxicity upon the cells,
198 hence excluded from the subsequent experiment.
199

Next, we intended to test whether the reduction in the luciferase activity of the reporter virus, as a result of pretreatment with Cu-Gr nanocomposite, can also be correlated to the reduction of progeny virus titer. A non-reporter variant of the influenza A/H1N1/WNS/1933 virus was used for this purpose. Virus stock solutions were either treated with two different concentrations of Cu-Gr nanocomposites (1µM and 5µM) or with the vehicle control prior to infection on MDCK cells. Plaque assay was performed to measure the titer of the progeny virus particles harvested at 8 hours of post-infection. There is about 40% decrease in viral titer for the sets treated 5uM Cu-Gr solution with respect to the vehicle treated sets. Treatment with 1µM Cu-Gr nanocomposite shows non-significant decrease in viral titer. This data further substantiates the fact that treatment with 5µM Cu-Gr significantly reduces viral infectivity which results in a decrease in viral gene expression, replication and subsequent production of viral titer (Figure 5C). The plaque assay titer data are tabulated in Figure 5D.

Prior treatment with Cu-Gr nanocomposite explicitly inhibits virus entry into the cells

At this point, we sought to examine the molecular mechanism by which Cu-Gr nanocomposite interferes with virus replication cycle. Metal nanoparticles have been shown to interfere with the integrity of the virus particles or the activity of the surface glycoproteins that may interfere with the entry of virus particles into the host cells (Sunada, Minoshima, and Hashimoto 2012) (Ting Du. 2018). Hence, to investigate the effect of pretreatment of Cu-Gr specifically upon virus entry step, we have performed an 'entry assay' (Figure 6A). The non-reporter variant of Influenza A WSN virus were either treated with Cu-Gr or with solvent and subsequently used to infect MDCK cells in a synchronized fashion. Post entry, cells were incubated with cycloheximide containing media for one hour to allow the import of the incoming viral ribonucleoprotein complexes (RNPs) into the nucleus. Subsequently, the incoming viral RNPs were stained with antibodies specific to viral Nucleoprotein (NP), which is the major component of the RNPs. As shown in the Figure 6 B, input viral RNPs are solely detected inside the nucleus of the infected cells irrespective of the treatment. However, prior exposure to the Cu-Gr composite resulted in a significant reduction in the number of NP positive cells. A quantitative analysis of 5 different fields with a total of 500 cells for both treated and untreated sets shows roughly 80% decrease in number of NP positive cells in the Cu-Gr treated set, with respect to the untreated one (Figure 6C). This data clearly suggests that exposure to Cu-Gr nanocomposite compromises the ability of the virus particles to enter into the host cell, possibly by impacting the structural integrity of the of the virion particles.

Development of a Cu-Gr nanocomposite based transparent coating with strong antiviral activity

The ability of Cu-Gr nanocomposite to reduce the infectivity of influenza A virus prompted us to test its ability to inactivate influenza virus in the solid form. For this purpose, we have coated different wells of a

48 well plate with a series of coating solutions containing different concentrations of Cu-Gr composite (1μM, 5μM, 10 μM and 20 μM) and polyvinyl alcohol (PVA) (1mm, 5mm, and 10mm) as a capping agent. As a control, wells were coated with only PVA. This process generated a thin transparent film of Cu-Gr nanocomposite onto the surface of each well. To test the antiviral activity of these films, defined amounts of Nano-Luc influenza A reporter virus were inoculated in these coated wells and incubated for 30 minutes. Post treatment, infectivity of these virus inoculums were tested on MDCK cells using the Nano-Luc reporter assay as mentioned above. Prior exposure to the coating materials having various concentrations of Cu-Gr composite blended in different amounts of PVA resulted in differential effects upon viral replication (Figure 7). Films containing different concentrations of Cu-Gr composite, either in absence or in presence 1mM PVA barely showed any impact upon the infectivity of the virus. In contrast, an exact dose-dependent decrease in viral gene expression was observed as a result of prior treatment with the films containing increasing concentrations of Cu-Gr Composite in 5mM PVA. This antiviral activity was even more pronounced (70% decrease in Nano-Luc activity) for the films containing 1-5uM of Cu-Gr with 10mM of PVA. Together, this data shows 5uM of Cu-Gr composite capped with 10mM of PVA could be used to generate a transparent coating with high antiviral activity.

Encouraged by the results mentioned above, we have used dip-coating method used to coat a tempered glass with the Cu-Gr solution with optimum concentration. The glass unit was kept to soak the solution for 24 h and then air-dried naturally as shown in (Figure 8A). No formation of visibly aggregated spots or clogging was observed on the glass surface. A clean, transparent screen was obtained, and when fixed on a cell phone, there was no compromisation of light intensity or clarity of image on the display screen observed (Figure 8B). Optical transmittance spectra confirm the transparency of the coating on glass substrates (Figure 8C). As observed from the SEM images (Figure 8D), the Cu-O nanoparticles were uniformly embedded on top of the graphene layer. Elemental analysis of Cu-Gr compounds was conducted by color mapping and EDAX analysis. The data presented in the right panel of Figure 8D and Figure 8E confirmed the presence of C, O, and Cu elements in the composites sample and their uniform distribution in the sample. Figure 8F shows a schematic representation of the Cu_2O and CuO nanoparticles embedded on the graphene sheets with PVA as a binding agent.

Discussions

RNA viruses constitute one of the broader families of human pathogens, including influenza, Nipah, Ebola, SARS or MERS-Coronaviruses. Irrespective of their specific differences in virus replication cycle, all of these viruses share broader structural similarities. The viral genomic RNA remains enwrapped with single or multiple viral proteins and remains enclosed within the lipid bilayer envelope embedded with viral spike

proteins. The integrity of the lipid envelope and the functionality of the spike proteins are not only crucial for the protection of the viral genomic materials in the outer environment but also indispensable for conducting the first two steps of the virus life cycle that are "attachment" and "entry" (Jane Flint, Vincent R 2015). In this study, we have identified Cu-Gr nanocomposite as a potential antiviral agent that can interfere with these two steps of the influenza A virus life cycle, possibly through compromising the structural integrity of the virion particles.

We, for the first time, have used a highly sensitive Nano-Luc reporter assay to perform an unbiased screening of a series of nanoparticles and their composite materials in order to identify a coating substance with strong antiviral activity. Our data identified Cu-Gr nanocomposite as the most potential antiviral agent. Interestingly, Cu nanoparticles or graphene individually showed minimal or no antiviral activity in our assay while a hybrid between these two showed at least ten-fold decrease in effective viral titer. This might be due to the property of the composite substances, which is not just a hybrid between two materials in their original state, but rather a combination of the modified version of the materials (Ramakrishnan et al. 2015). This can also be substantiated from the previous studies showing metal-ion based composites shows better activity compared to that of metal nanoparticles itself (Minoshima et al. 2016; Perdikaki et al. 2018; Sunada, Minoshima, and Hashimoto 2012). Studies also reveal that the antiviral activity mainly depends on the presence of ions generated from the surface of nanoparticles (Ma et al. 2011) (Shen et al. 2010). Our XRD data clearly indicates the presence of various copper oxide species, Cu_2O and CuO, embedded in the graphene sheets which may serve as the basis for the antiviral activity of the composite material. The presence of reactive oxygen species in Cu_xO-graphene sheets may provide ions, which may interfere with the structural integrity of the lipid bilayer membrane or the surface antigens of the virion particles. This interference should compromise the ability of the virus particles to interact with the cell surface receptor essential for the attachment and subsequent entry into the host cell. Our entry assay supports this hypothesis, as prior treatment with Cu-Gr composite resulted in significant reduction in the percentage of infection positive cells with respect to the vehicle treated set.

Finally, we have used PVA as a capping agent and identified optimum concentrations of Cu-Gr and PVA to develop a thin transparent coating with intense antiviral activity. While we have used dip-coating method to coat a tempered glass with high visibility, other forms of coatings like doctor's blade technique, spin coating, and spray coating can also be implemented. Due to the high transmission efficiency, such coating material could be implemented on a wide variety of surfaces, which could radically decrease the stability of the virus particles in the outer environment and hence reduce the transmission rate drastically. Needless to mention that such generic antiviral strategy can significantly reduce the overall burden of seasonal

299 respiratory infection-related epidemics or occasional pandemics caused either by various influenza or
300 coronaviruses.

301 **Materials and Methods**

302 **Chemicals**:

303 Copper sulfate ($CuSO_4$ > 99%), Silver nitrate ($AgNO_3$ > 99%), Sodium borohydride ($NaBH_4$ > 98%), Poly
304 vinyl alcohol (>99%), Sodium hydroxide pellets (NaOH > 97%) and graphite powder (>98%) were
305 purchased from Sigma-Aldrich.

306

307 **Cells, Viruses and Antibody:** Madin Darby Canine Kidney (MDCK) (CCL-34) cells were maintained in
308 Dulbecco's modified Eagle's medium (DMEM) supplemented with 5% FBS at 37˚C and 5% CO_2 along
309 with penicillin and streptomycin antibiotics (Gibco).

310

311 Influenza A virus strains, A/WSN/1933 (H1N1), WSN stably encoding PB2 with a C-terminal FLAG tag
312 (WSN-PB2-FLAG) (Dos Santos Afonso et al. 2005) or PA-2A-Swap-Nluc (PASTN) reporter virus based
313 on the strain A/WSN/33 (H1N1) were used for infecting the cells (Tran et al. 2013). Antibody used
314 includes anti-NP (H16-L10-4R5) (Yewdell et al., 1981).

315

316 **Synthesis of materials:**

317 Initially, the graphene dispersion was prepared using a liquid exfoliation of the graphite powder in
318 Deionized (DI) water (20 mg/300 mL) using an ultrasonic probe sonicator. Probe sonication of frequency
319 30 Hz was used in pulses for 2 hours. Silver (Ag) and Copper (Cu) stock solutions were prepared using
320 4mM $AgNO_3$ (68 mg/100 mL) and 4 mM $CuSO_4$ (63.8 mg/100 mL) in DI water medium respectively.
321 Graphene solution (45 mL) was mixed with 15 mL of Cu and Ag stock solution separately by maintaining
322 the pH=12 adjusted through NaOH. 20 mL of 4 mM $NaBH_4$ (30 mg/200 mL) solution, a strong reducing
323 agent is added drop wise with the Cu-graphene (Cu-Gr), Ag-graphene (Ag-Gr) and Cu-Ag-graphene (Cu-
324 Ag-Gr) mixtures separately and stirred continuously at 40^0C.
325 Furthermore, four different concentrations (1µM, 5µM, 10µM and 20µM) of Cu functionalized graphene
326 samples were synthesized for biological process optimization. Three different concentrations (1mM, 5mM
327 and10mM) of poly vinyl alcohol have been capped as a coating media for the Cu-graphene samples.

328

329 **Material characterizations:**

330 Different phases of the synthesized sample (Cu functionalized graphene) were obtained from the X-ray
331 diffraction (XRD) peaks by using Bruker D8 Advance X-ray diffractometer within a scan range of 2Theta

(2θ) values 7 and 90° with Cu-Kα source, maintaining the scan rate of 1° min^{-1}. Absorption spectra of Cu-graphene synthesized sample were recorded by a BioTek UV-vis spectrophotometer Epoch 2 microplate within 200 nm to 800 nm wavelength. Raman shifts were measured by using WiTec –alpha 300R confocal microscope at excitation of 532 nm in the wavenumber range of 200 cm^{-1} to 3000 cm^{-1}. SEM images were obtained through Zeiss-Merlin EVO 60 scanning electron microscope with Oxford EDS detector.

MTT assay:

MDCK cells were seeded in 96 well plates at a density of 15000 cells per well. The cells were treated with Silver (Ag), Graphene (Gr), Copper (Cu) nanoparticles as well as Ag-Gr, Cu-Gr and Ag-Cu-Gr nanocomposites respectively for 24 hours (h) at 37°C in 5% CO_2. Cellular cytotoxicity assay was performed according to the manufacturer's protocol. In brief, after 24 h of treatment with the nanoparticle, 100µl of MTT reagent (5 mg/ml, SRL) in PBS was added to the cells and incubated for 3 h at 37°C. The medium was removed carefully without disturbing the formazan crystals and 100µl of DMSO (Sigma) was added to dissolve the insoluble purple formazan crystals. The absorbance of the suspension was measured at 595 nm using Epoch 2 Microplate Reader (BioTek instruments). The percentages of metabolically active cells were compared with the percentage of control cells of the same culture plate as a proxy for cell viability. Cellular cytotoxicity was determined in triplicate and each experiment was repeated three times independently.

Nano-Luc reporter assay:

The Nano-Luc reporter assay was used to determine the luciferase activity as previously mentioned by Tran et al., 2013 (Tran et al. 2013). MDCK cells seeded in a 96 well plate were infected in triplicate with the Nano Luciferase influenza A reporter virus, PASTN. Accordingly, the virus was preincubated with a particular concentration of the nanoparticle/nanocomposite for 30 min or mentioned otherwise. The vehicle control or the nanoparticle/ nanocomposite treated virus was used to infect MDCK cells. The infected cells were harvested at 8hpi and the viral NLuc activity was measured by using Nano-Glo® Luciferase Assay System according to the manufacturer's instructions (Promega) and the luminescence was detected by using a Luminometer (Glomax 20/20, Promega).

Plaque assay:

A non-reporter variant of the influenza A/H1N1/WSN/1933 virus stock solutions MOI 0.1 was either preincubated with vehicle control or Cu-Gr nanocomposite (1uM and 5uM) followed by infection in MDCK cells. At 8hpi, the viral supernatant was collected and used to reinfect MDCK cells and plaque assay was

365 performed to determine the progeny viral titer followed by Matrosovich M, 2006 (Matrosovich et al. 2006).
366 Accordingly, after 1 hr of infection with the virus, cells were overlaid with a media containing a mixture of
367 2X DMEM and 2.4% avicel (1:1 ratio). After 62hrs, the overlay was discarded and the cells were fixed with
368 70% ethanol followed by staining with 2% Crystal violet. Plaques were counted and plaque forming unit
369 (PFU/ml) was calculated to measure the progeny viral titer.
370
371 **Viral entry assay:**
372 MDCK cells grown on coverslips were infected with vehicle control or 5uM Cu-Gr treated virus at a MOI
373 of 5. Viral entry assay was performed according to the protocol followed by Mondal et al., 2017 (Mondal
374 et al. 2017). Virion binding was performed at 4˚C for 1hr in presence of 1mM of Cycloheximide, CHX
375 (Sigma). The viral inoculum was washed off with cold PBS to remove unbound virus particles. Thereafter,
376 the prewarmed virus growth media (VGM, containing DMEM, 0.2% bovine serum albumin (BSA), 25 mM
377 HEPES buffer, and 0.5 mg/ml TPCK-trypsin) supplemented with 1mM of CHX was added to the cells and
378 synchronous infection was initiated by shifting cells to 37˚C. At 1 hpi, cells were fixed with 3%
379 formaldehyde and permeabilized with 0.1M Glycine/0.1% Triton-X 100 in PBS for 20 min at room
380 temperature. Blocking was performed at 4˚C with 3% BSA overnight. NP was detected with anti-NP
381 antibody and Alexa Fluor 555-conjugated donkey anti-mouse IgG antibody (Invitrogen). DAPI (Sigma)
382 was used to stain the nucleus. Cells were imaged using Fluorescent microscope (Leica Microsystems) and
383 image analysis was performed with ImageJ software.
384
385 **Statistics:**

386 Each data is a representative of at least three independent experiments, each experiment was performed in
387 triplicate. Graphs are performed in Microsoft Excel and represented as mean standard deviations (n=3).
388 Results were compared by performing two-tailed Student's t test. Significance is defined as $p<0.05$ and
389 statistical significance is indicated with an asterisk (*). The *p value < 0.05, **p value < 0.01 **p value
390 and ***p < 0.001 were considered statistically significant.
391
392 **Acknowledgement:**
393
394 We sincerely thank Prof. Andrew Mehle, University of Wisconsin Madison, for providing the Nano-Luc
395 influenza A reporter viruses. This work was primarily supported by Sponsored Research and Industrial
396 Consultancy (SRIC) IIT Kharagpur. AM would like to thank DBT for Ramalingaswami re-entry fellowship,
397 SERB for Early Career Research Award and MHRD for the "Scheme for Transformational and Advanced
398 Research in Science" for additional financial support.

399
400
401
402 **References**

403 Barani, Zahra et al. 2020. "Thermal Properties of the Binary-Filler Hybrid Composites with Graphene and
404 Copper Nanoparticles." *Advanced Functional Materials* 30(8): 1–11.
405 Chan, George H. et al. 2007. "Plasmonic Properties of Copper Nanoparticles Fabricated by Nanosphere
406 Lithography." *Nano Letters* 7(7): 1947–52.
407 Cioffi, Nicola et al. 2005. "Copper Nanoparticle/Polymer Composites with Antifungal and Bacteriostatic
408 Properties." *Chemistry of Materials* 17(21): 5255–62.
409 Darabdhara, Gitashree et al. 2017. "Cu-Ag Bimetallic Nanoparticles on Reduced Graphene Oxide
410 Nanosheets as Peroxidase Mimic for Glucose and Ascorbic Acid Detection." *Sensors and Actuators,*
411 *B: Chemical* 238: 842–51.
412 Deng, Dunying et al. 2013. "Copper Nanoparticles: Aqueous Phase Synthesis and Conductive Films
413 Fabrication at Low Sintering Temperature." *ACS Applied Materials and Interfaces* 5(9): 3839–46.
414 Deng, Yilin et al. 2016. "In Situ Raman Spectroscopy of Copper and Copper Oxide Surfaces during
415 Electrochemical Oxygen Evolution Reaction: Identification of CuIII Oxides as Catalytically Active
416 Species." *ACS Catalysis* 6(4): 2473–81.
417 Edwards, Rebecca S., and Karl S. Coleman. 2013. "Graphene Synthesis: Relationship to Applications."
418 *Nanoscale* 5(1): 38–51.
419 Eigler, Siegfried, and Andreas Hirsch. 2014. "Chemistry with Graphene and Graphene Oxide -
420 Challenges for Synthetic Chemists." *Angewandte Chemie - International Edition* 53(30): 7720–38.
421 Fehr, Anthony R, and Stanley Perlman. 2015. "Coronaviruses: An Overview of Their Replication and
422 Pathogenesis." *Methods in molecular biology (Clifton, N.J.)* 1282: 1–23.
423 Ferrari, A. C. et al. 2006. "Raman Spectrum of Graphene and Graphene Layers." *Physical Review Letters*
424 97(18): 1–4.
425 Gawande, Manoj B. et al. 2016. "Cu and Cu-Based Nanoparticles: Synthesis and Applications in
426 Catalysis." *Chemical Reviews* 116(6): 3722–3811.
427 Georgakilas, Vasilios et al. 2012. "Functionalization of Graphene: Covalent and Non-Covalent
428 Approach." *Chemical Reviews* 112(11): 6156–6214.
429 Hang, Xiaofeng et al. 2015. "Antiviral Activity of Cuprous Oxide Nanoparticles against Hepatitis C Virus
430 in Vitro." *Journal of Virological Methods* 222: 150–57.
431 http://dx.doi.org/10.1016/j.jviromet.2015.06.010.
432 Hu, Yanjie et al. 2013. "Scalable Preparation of Ultrathin Silica-Coated Ag Nanoparticles for SERS

433 Application." *ACS Applied Materials and Interfaces* 5(21): 10643–49.
434 Jane Flint, Vincent R, Glen F Rall and Anna Marie with Lynn W Enquist. 2015. *Principles of Virology,*
435 *4th Edition*.
436 Jin, Rongchao, Justin E. Jureller, Hee Y. Kim, and Norbert F. Scherer. 2005. "Correlating Second
437 Harmonic Optical Responses of Single Ag Nanoparticles with Morphology." *Journal of the*
438 *American Chemical Society* 127(36): 12482–83.
439 Johnson, Niall P.A.S., and Juergen Mueller. 2002. "Updating the Accounts: Global Mortality of the 1918-
440 1920 'Spanish' Influenza Pandemic." *Bulletin of the history of medicine* 76(1): 105–15.
441 Karahan, Hüseyin Enis et al. 2018. "Graphene Materials in Antimicrobial Nanomedicine: Current Status
442 and Future Perspectives." *Advanced Healthcare Materials* 7(13): 1–18.
443 Kim, Un Jeong et al. 2018. "Anomalous K-Point Phonons in Noble Metal/Graphene Heterostructure
444 Activated by Localized Surface Plasmon Resonance." *ACS Nano* 12(12): 12733–40.
445 Koven, S. 2020. "Engla, Journal - 2010 - New Engla Nd Journal." *New England Journal of Medicine*: 1–
446 2.
447 Landrigan, Philip J. et al. 2018. "The Lancet Commission on Pollution and Health." *The Lancet*
448 391(10119): 462–512.
449 Letko, Michael, Andrea Marzi, and Vincent Munster. 2020. "Functional Assessment of Cell Entry and
450 Receptor Usage for SARS-CoV-2 and Other Lineage B Betacoronaviruses." *Nature Microbiology*
451 5(4): 562–69.
452 Lin, Leon Chien Wei et al. 2019. "Viromimetic STING Agonist-Loaded Hollow Polymeric Nanoparticles
453 for Safe and Effective Vaccination against Middle East Respiratory Syndrome Coronavirus."
454 *Advanced Functional Materials* 29(28): 1–15.
455 Ma, Jizhen et al. 2011. "Preparation, Characterization and Antibacterial Properties of Silver-Modified
456 Graphene Oxide." *Journal of Materials Chemistry* 21(10): 3350–52.
457 Matrosovich, Mikhail, Tatyana Matrosovich, Wolfgang Garten, and Hans Dieter Klenk. 2006. "New
458 Low-Viscosity Overlay Medium for Viral Plaque Assays." *Virology Journal* 3: 1–7.
459 Minoshima, Masafumi et al. 2016. "Comparison of the Antiviral Effect of Solid-State Copper and Silver
460 Compounds." *Journal of Hazardous Materials* 312: 1–7.
461 Mohammed, Hiba et al. 2020. "Antimicrobial Mechanisms and Effectiveness of Graphene and Graphene-
462 Functionalized Biomaterials. A Scope Review." *Frontiers in Bioengineering and Biotechnology*
463 8(May).
464 Mondal, Arindam et al. 2017. "Influenza Virus Recruits Host Protein Kinase C to Control Assembly and
465 Activity of Its Replication Machinery." *eLife* 6: 1–23.
466 Neeltje van Doremalen, PhD et al. 2020. "Aerosol and Surface Stability of SARS-CoV-2 as Compared

with SARS-CoV-1." *New England Journal of Medicine*: 0–2.

Novoselov, K. S. et al. 2012. "A Roadmap for Graphene." *Nature* 490(7419): 192–200. http://dx.doi.org/10.1038/nature11458.

Palmieri, V., and M. Papi. 2020. "Can Graphene Take Part in the Fight against COVID-19?" *Nano Today* 33: 100883.

Park, Se Jin et al. 2020. "Discovery of Direct-Acting Antiviral Agents with a Graphene-Based Fluorescent Nanosensor." *Science Advances* 6(22): 1–12.

Patterson, David, and Gerald Pyle. 2019. "The Geography and Mortality of the 1918 Influenza Pandemic." *Bulletin of the History of Medicine* 65(1): 4–21.

Perdikaki, Anna et al. 2018. "Ion-Based Metal/Graphene Antibacterial Agents Comprising Mono-Ionic and Bi-Ionic Silver and Copper Species." *Langmuir* 34(37): 11156–66.

Ramakrishnan, S. et al. 2015. "One-Step Synthesis of Pt-Decorated Graphene-Carbon Nanotubes for the Electrochemical Sensing of Dopamine, Uric Acid and Ascorbic Acid." *Analytical Methods* 7(2): 779–86.

Ruparelia, Jayesh P., Arup Kumar Chatterjee, Siddhartha P. Duttagupta, and Suparna Mukherji. 2008. "Strain Specificity in Antimicrobial Activity of Silver and Copper Nanoparticles." *Acta Biomaterialia* 4(3): 707–16.

Dos Santos Afonso, Emmanuel et al. 2005. "The Generation of Recombinant Influenza A Viruses Expressing a PB2 Fusion Protein Requires the Conservation of a Packaging Signal Overlapping the Coding and Noncoding Regions at the 5′ End of the PB2 Segment." *Virology* 341(1): 34–46.

Saunders-Hastings, Patrick R., and Daniel Krewski. 2016. "Reviewing the History of Pandemic Influenza: Understanding Patterns of Emergence and Transmission." *Pathogens* 5(4).

Shen, Jianfeng et al. 2010. "Facile Synthesis and Application of Ag-Chemically Converted Graphene Nanocomposite." *Nano Research* 3(5): 339–49.

Sunada, Kayano, Masafumi Minoshima, and Kazuhito Hashimoto. 2012. "Highly Efficient Antiviral and Antibacterial Activities of Solid-State Cuprous Compounds." *Journal of Hazardous Materials* 235–236: 265–70. http://dx.doi.org/10.1016/j.jhazmat.2012.07.052.

Taubenberger, Jeffery K., and David M. Morens. 2006. "1918 Influenza: The Mother of All Pandemics." *Emerging Infectious Diseases* 12(1): 15–22.

Ting Du., et al. 2018. "Antiviral Activity of Graphene Oxide−Silver Nanocomposites_2018.Pdf."

Tran, V., L. A. Moser, D. S. Poole, and A. Mehle. 2013. "Highly Sensitive Real-Time In Vivo Imaging of an Influenza Reporter Virus Reveals Dynamics of Replication and Spread." *Journal of Virology* 87(24): 13321–29.

Vasickova, P, I Pavlik, M Verani, and A Carducci. 2010. "Issues Concerning Survival of Viruses on

Surfaces." *Food and Environmental Virology* 2(1): 24–34.

Vinothini, Kandasamy, and Mariappan Rajan. 2017. "Investigation on the Use of Graphene as a Unique Drug Delivery Platform for Dissimilar Anticancer Drugs." *Progress in Bioscience and Bioengineering* 1(1): 11–17.

De Wit, Emmie, Neeltje Van Doremalen, Darryl Falzarano, and Vincent J. Munster. 2016. "SARS and MERS: Recent Insights into Emerging Coronaviruses." *Nature Reviews Microbiology* 14(8): 523–34.

World Health Organization. 2018. "The Top 10 Causes of Death." *World Health Organization*.

Wu, Jiang Bin et al. 2018. "Raman Spectroscopy of Graphene-Based Materials and Its Applications in Related Devices." *Chemical Society Reviews* 47(5): 1822–73.

Wu, Yuntao et al. 2020. "SARS-CoV-2 Is an Appropriate Name for the New Coronavirus." *The Lancet* 395(10228): 949–50.

Yao, Wei Tang et al. 2005. "Formation of Uniform CuO Nanorods by Spontaneous Aggregation: Selective Synthesis of CuO, Cu2O, and Cu Nanoparticles by a Solid-Liquid Phase Arc Discharge Process." *Journal of Physical Chemistry B* 109(29): 14011–16.

Ye, Shiyi et al. 2015. "Antiviral Activity of Graphene Oxide: How Sharp Edged Structure and Charge Matter." *ACS Applied Materials and Interfaces* 7(38): 21578–79.

Zhang, Zhuanfang et al. 2020. "Facile Hydrothermal Synthesis of CuO-Cu2O/GO Nanocomposites for the Photocatalytic Degradation of Organic Dye and Tetracycline Pollutants." *New Journal of Chemistry* 44(16): 6420–27.

Ziem, Benjamin et al. 2016. "Highly Efficient Multivalent 2D Nanosystems for Inhibition of Orthopoxvirus Particles." *Advanced Healthcare Materials* 5(22): 2922–30.

Figure legends

Figure 1. Different nanoparticles and their nanocomposites. (A) Digital photographs of all the synthesized nanoparticle and nanocomposite samples. (B) Schematic representation of the Cu and Ag nanoparticles embedded two dimensional graphene sheets. (C-D) UV-Vis absorption spectra of synthesized nanoparticles and their composites.

Figure 2. Nanoparticles and nanocomposites shows minimal cytotoxicity. MDCK cells were either treated with vehicle control or different concentrations (0.5, 1, 5 μM) of the Ag, Cu and Gr nanoparticles or Ag-Gr, Cu-Gr and Ag-Cu-Gr nanocomposites for 24 h and their cytotoxicity were determined by MTT assay. Cellular cytotoxicity was determined in triplicate and each experiment was repeated three times. Data are presented as means ± standard deviations (SD) (n=3).

Figure 3. Screening of different the nanoparticles/ nanocomposites for antiviral activity using Nano-Luciferase influenza A reporter. (A) MDCK cells were infected with different amounts (0.01-0.1) of Nano-Luciferase Influenza A reporter virus and the reporter activity was measured using Nano glo reporter assay (Promega). To demonstrate the relationship between the MOI and luciferase activity (arbitrary unit) was plotted as a function of MOI. (B) To test the antiviral activity, the Influenza A reporter virus was pretreated with the 5uM colloidal suspensions of each of the materials for 30 minutes at RT and followed by infection of MDCK cells at MOI of 0.1as diagrammed. (C) Luciferase activity of the nanoparticle/ nanocomposite treated sets were measured at 8 hpi and plotted as a relative percentage of the vehicle treated set. For all experiments, data are mean of n=3± standard deviation (*, P< 0.05; n=3 ± sd).

Figure 4. Material characterization of the Cu-Gr nanocomposite. (A) Raman spectrum of Cu-Gr nanocomposites. Inset shows optical microscopy image of the composite and Raman spectrum of Cu_xO. (B) XRD spectrum of composites sample confirming the presence of CuO, Cu_2O, and Graphene.

Figure 5. Prior incubation with Cu-Gr nanocomposite severely impacts the infectivity of influenza A virus. (A) A time kinetics experiment was performed by treating Influenza A reporter virus with 5uM colloidal suspensions of Cu-Gr for 15, 30, 45 and 60 min at RT and followed by infection of MDCK cells at MOI 0.1. Absolute luciferase activity values w.r.t viral gene expression for the vehicle and Cu-Gr treated sets are represented by black and grey bars respectively. (B) MDCK cells were infected with Influenza A reporter virus pretreated with vehicle or with different concentrations of the Cu-Gr composite (50nM, 100nM, 500nM, 1uM, 2uM and 5uM respectively). Viral gene expression was monitored using luciferase activity assay. Data were normalized to vehicle control sets for each nanoparticle. (C, D) A non-reporter A/H1N1/WSN/1933 influenza virus was either treated with Cu-Gr composite (1uM and 5uM) or with vehicle control prior to infecting MDCK cells. Plaque assay was performed to measure the titer of the progeny virus particles harvested at 8hpi. Percentage reduction in viral titers and actual PFUs for all experiments are represented. For all experiments, data are mean of n=3± standard deviation (*, P< 0.05; n=3 ± sd).

Figure 6. Cu-Gr interferes with the entry of Influenza A virus inside the cells. (A) Schematic depiction of Entry assay: MDCK cells were infected with influenza A virus either pretreated with 5uM Cu-Gr or with vehicle control. Synchronous infection was carried out by incubating the virus inoculum with the cell monolayer at 4^0C for one hour, followed by adding the virus growth media (VGM) supplemented with cycloheximide and prewarmed at 37^0C. Cells were incubated further for one hour before processing them for imaging (B) Intracellular localization of viral NPs in control and Cu-Gr treated sets were determined by staining with anti NP antibody and Alexa Fluor 555 (red). DAPI was used to stain the nucleus (Blue). (C)

570 Percentage of NP positive cells in control and in treated sets were analyzed using image J software and
571 depicted by bar diagram. For all experiments, data are mean of n=5± standard deviation (*, P< 0.05).

572 **Figure 7. PVA based Cu-Gr nanocomposite coating shows strong antiviral activity.** Different wells of
573 a 48 well plate was coated with coating solutions having different concentrations of Cu-Gr composite (1uM,
574 5 uM, 10 uM and 20 uM) and polyvinyl alcohol (PVA) (1mM, 5mM and 10mM). Nano Luciferase-
575 Influenza A virus (MOI 0.1) were inoculated in these wells and incubated for 30 minutes. Post treatment,
576 MDCK cells were infected with the viral inoculum recovered from the coated wells and luciferase activity
577 was determined at 8 hpi using Nano-Glo reporter assay (Promega). Luciferase activity of each set was
578 plotted as a relative percentage of the vehicle treated set. Each data was represented in triplicate and each
579 experiment was repeated three times. Data are presented as means ± standard deviations (SD) (n=3) (*, P<
580 0.05).
581

582 **Figure 8**. **PVA based Cu-Gr nanocomposite can be used to generate a highly transparent antiviral**
583 **coating of the cell phone screen.** (A) Schematic diagram of the deep coating method of tempered glass
584 unit with the PVA based Cu-Gr nanocomposite. (B) Transparency of dip coated tempered mobile screen.
585 (C) Transmittance spectrum of the coated sample. (D) SEM image of Cu-Graphene composites sample.
586 Right panel shows the color mapping of all elements. (E) EDX spectra of composites sample, confirm the
587 presence of Cu, C and O atoms. (F) Schematic representation of the composite structure.
588

589
590
591
592
593
594
595
596
597
598
599
600
601

Figure 1

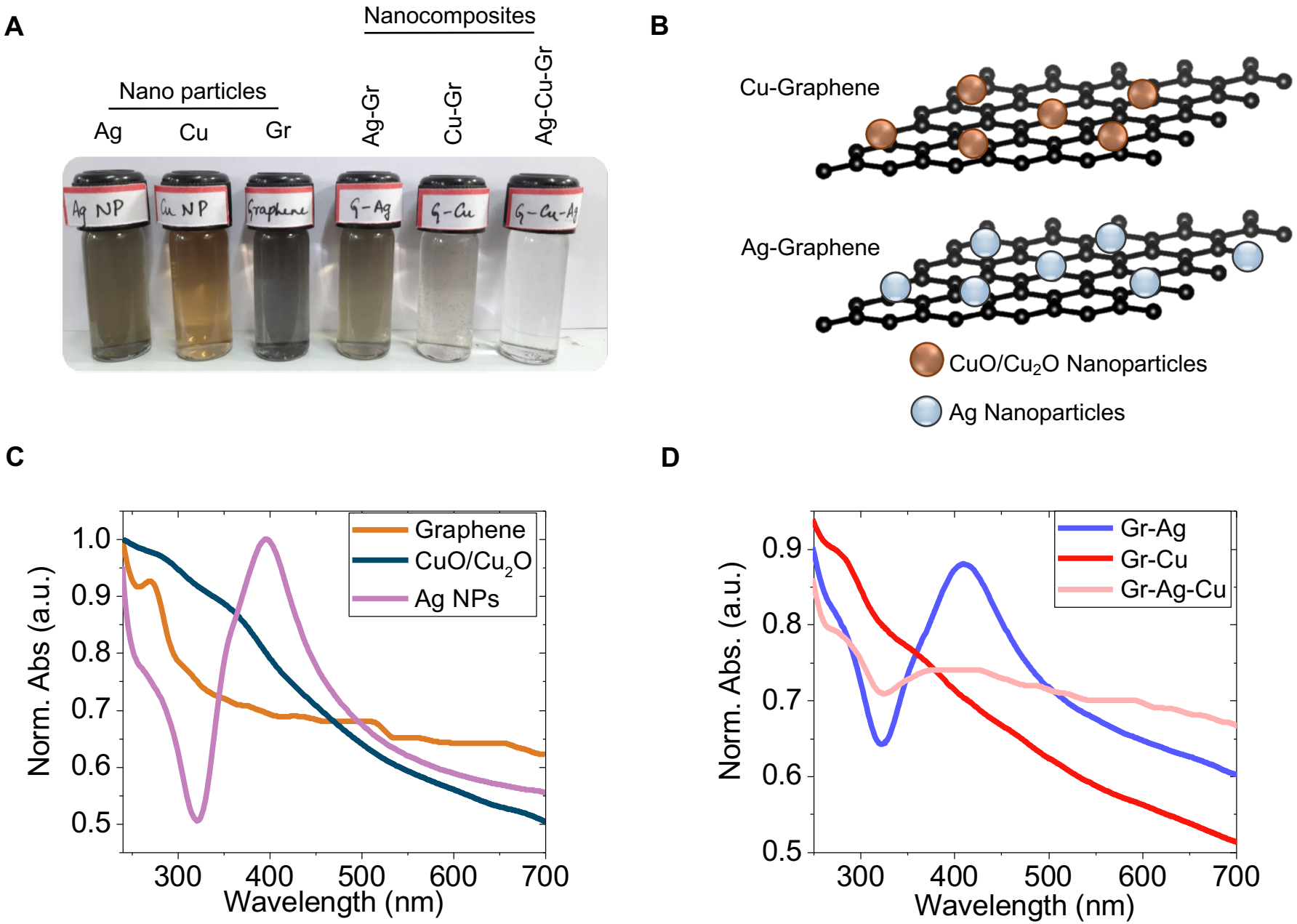
A
Nanocomposites
Nano particles
Ag
Cu
Gr
Ag-Gr
Cu-Gr
Ag-Cu-Gr
Ag NP
Cu NP
Graphene
G-Ag
G-Cu
G-Cu-Ag
B
Cu-Graphene
Ag-Graphene
CuO/Cu2O Nanoparticles
Ag Nanoparticles
C
Graphene
CuO/Cu2O
Ag NPs
Norm. Abs (a.u.)
Wavelength (nm)
D
Gr-Ag
Gr-Cu
Gr-Ag-Cu
Norm. Abs. (a.u.)
Wavelength (nm)

Figure 2

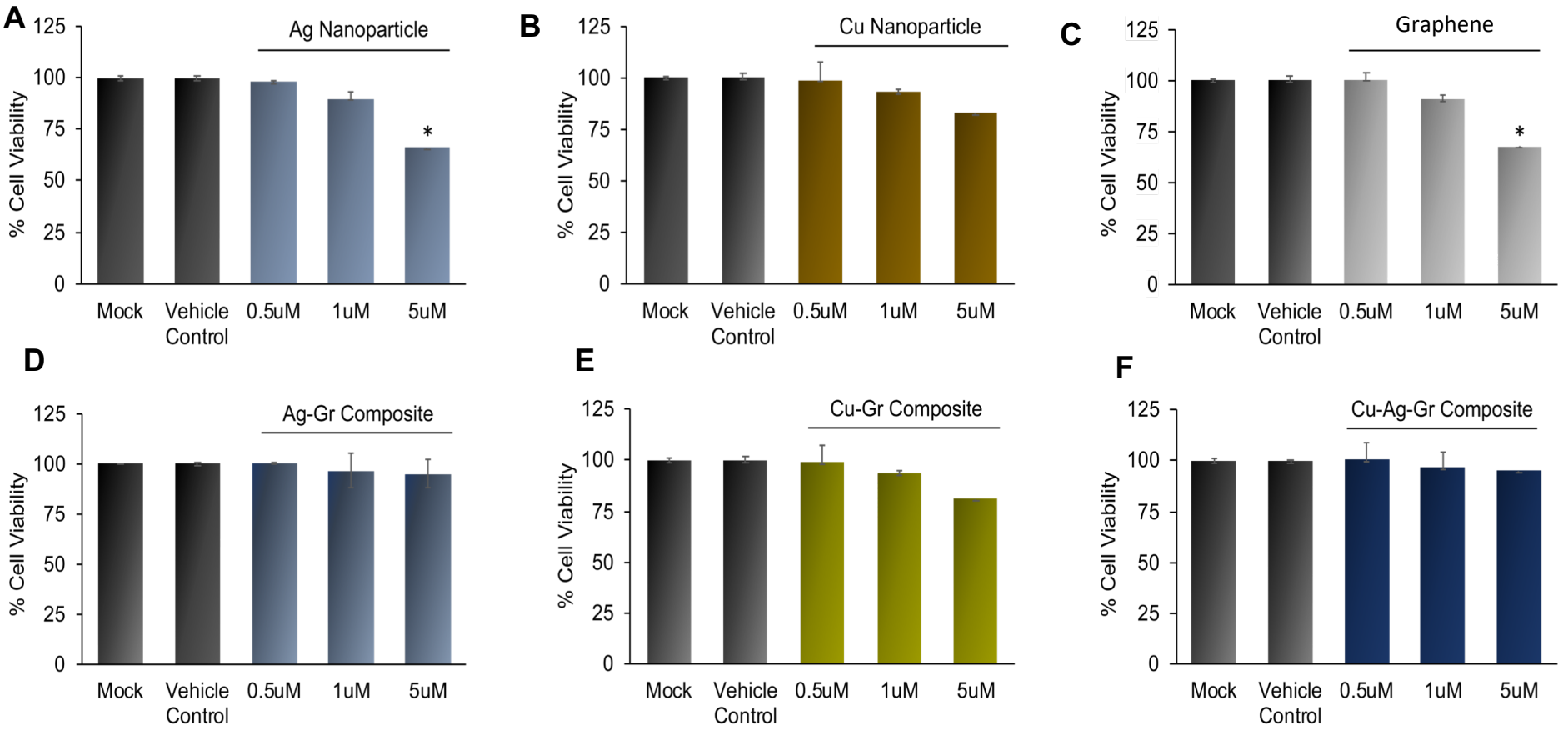
A
Ag Nanoparticle
B
Cu Nanoparticle
C
Graphene
D
Ag-Gr Composite
E
Cu-Gr Composite
F
Cu-Ag-Gr Composite
% Cell Viability
125
100
75
50
25
0
*
Mock
Vehicle Control
0.5uM
1uM
5uM

Figure 3

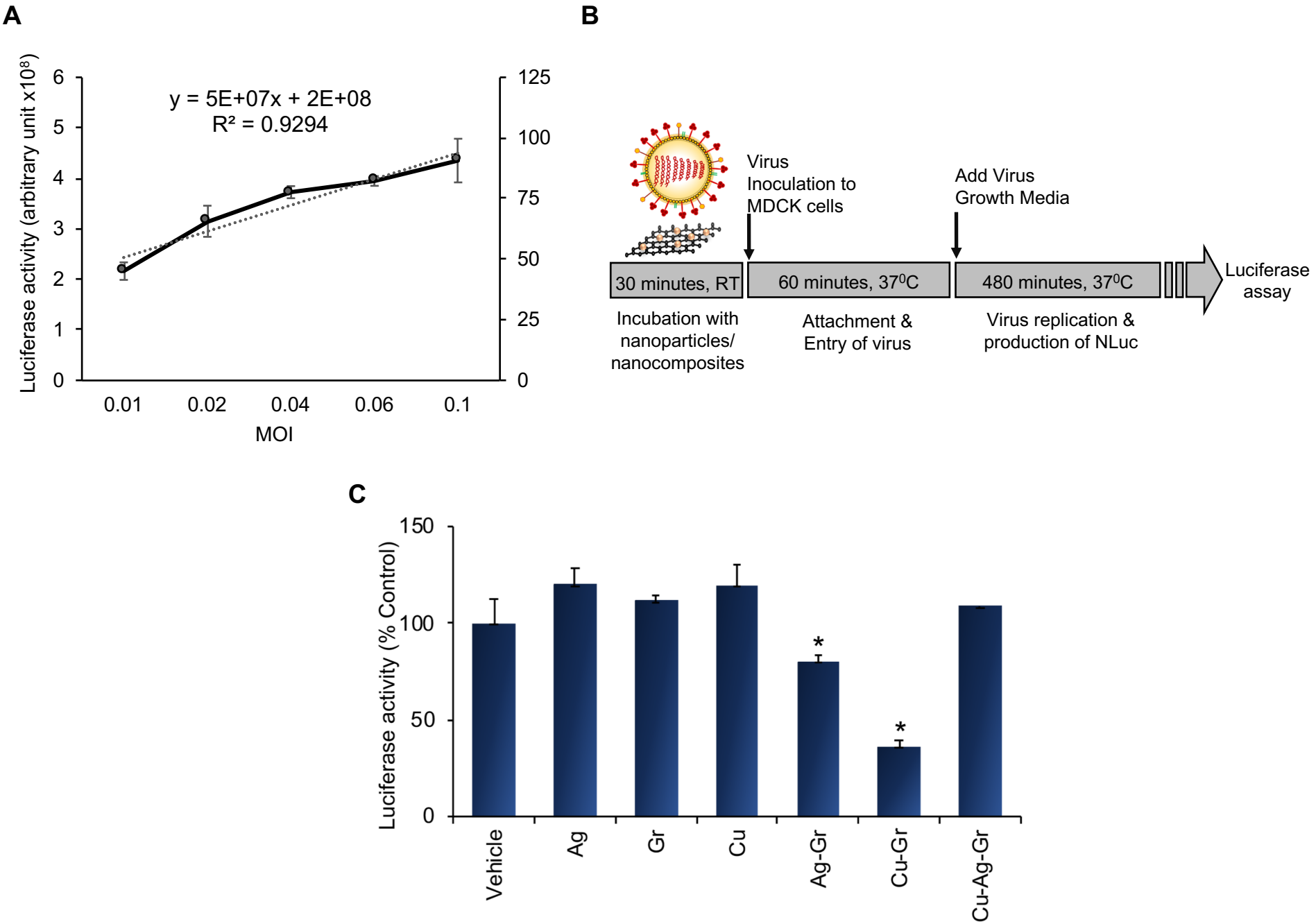
A
Luciferase activity (arbitrary unit x10⁸)
y = 5E+07x + 2E+08
R² = 0.9294
MOI
0.01
0.02
0.04
0.06
0.1
B
Virus Inoculation to MDCK cells
Add Virus Growth Media
30 minutes, RT
60 minutes, 37⁰C
480 minutes, 37⁰C
Luciferase assay
Incubation with nanoparticles/ nanocomposites
Attachment & Entry of virus
Virus replication & production of NLuc
C
Luciferase activity (% Control)
Vehicle
Ag
Gr
Cu
Ag-Gr
Cu-Gr
Cu-Ag-Gr

Figure 4

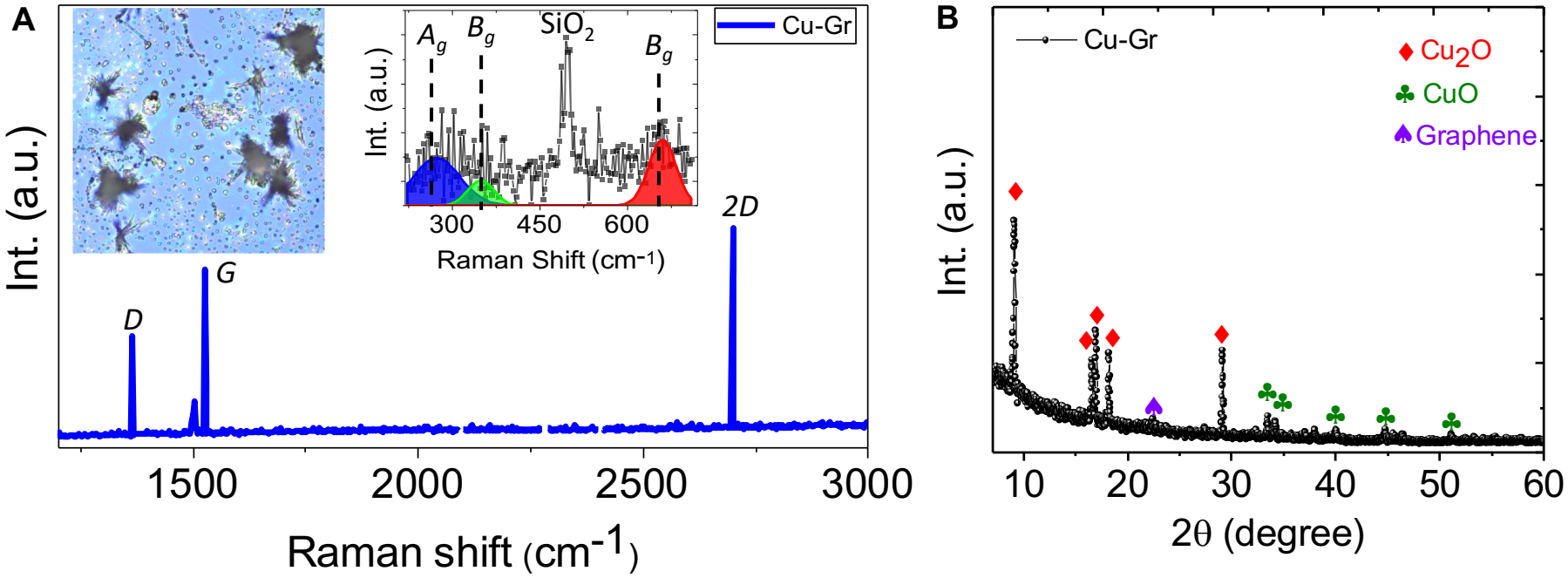
A
Int. (a.u.)
D
G
2D
1500
2000
2500
3000
Raman shift (cm-1)
Cu-Gr
Ag
Bg
SiO2
Bg
Int. (a.u.)
300
450
600
Raman Shift (cm-1)
B
Cu-Gr
Cu2O
CuO
Graphene
Int. (a.u.)
10
20
30
40
50
60
2θ (degree)

Figure 5

A

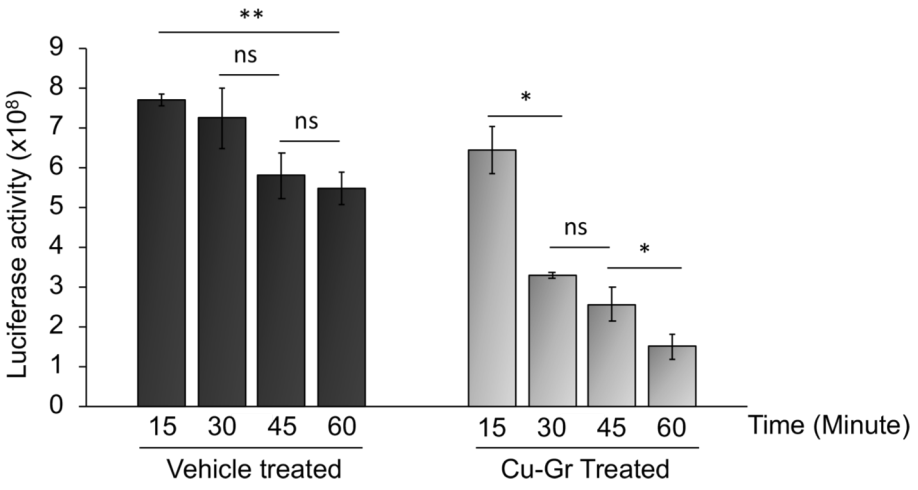

B

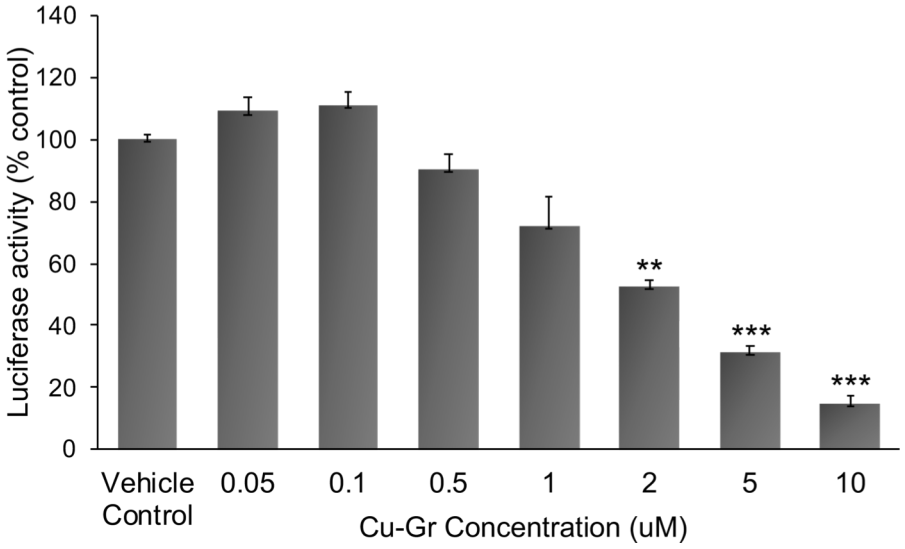

C

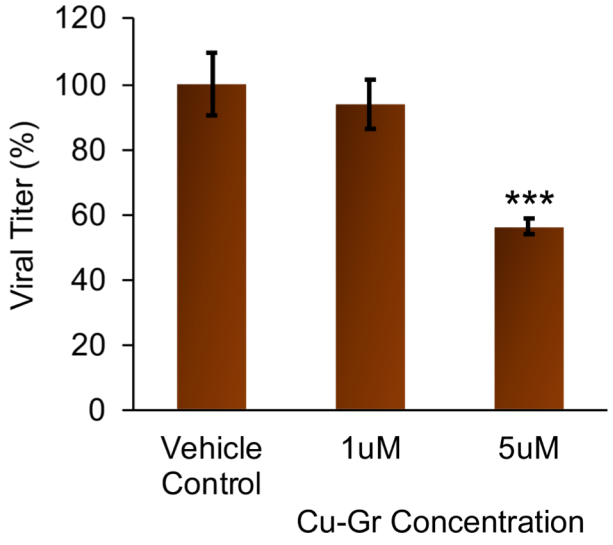

D

	Viral titer (Pfu/ml)		
	Replicate-1	Replicate-2	Replicate-3
Vehicle Control	57000	50000	55000
Cu-Gr 1uM	54000	48000	50000
Cu-Gr 5uM	29000	31000	31000

Figure 6

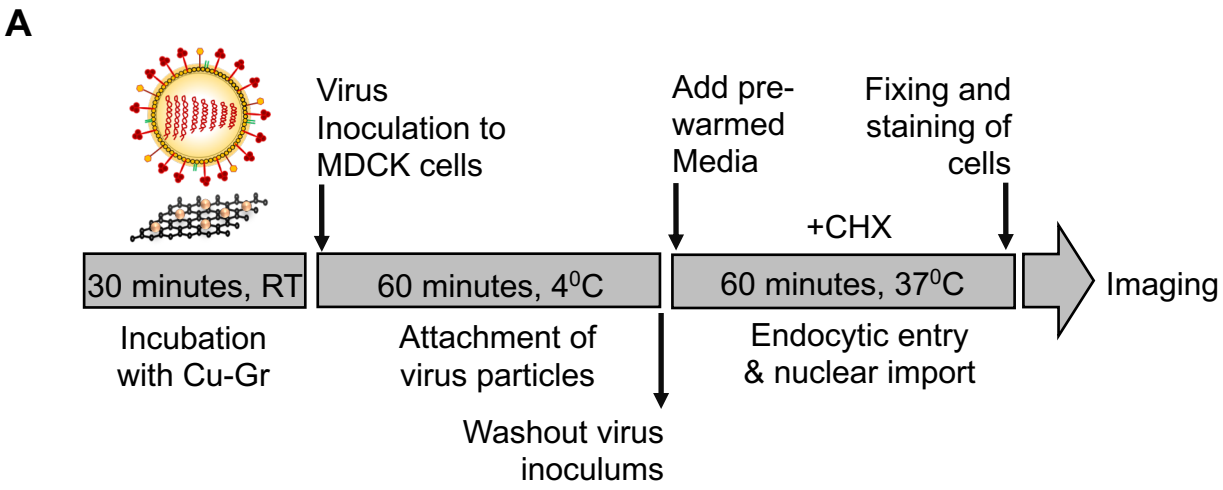
A
Virus
Inoculation to
MDCK cells
Add pre-
warmed
Media
Fixing and
staining of
cells
+CHX
30 minutes, RT
60 minutes, 4⁰C
60 minutes, 37⁰C
Imaging
Incubation
with Cu-Gr
Attachment of
virus particles
Endocytic entry
& nuclear import
Washout virus
inoculums

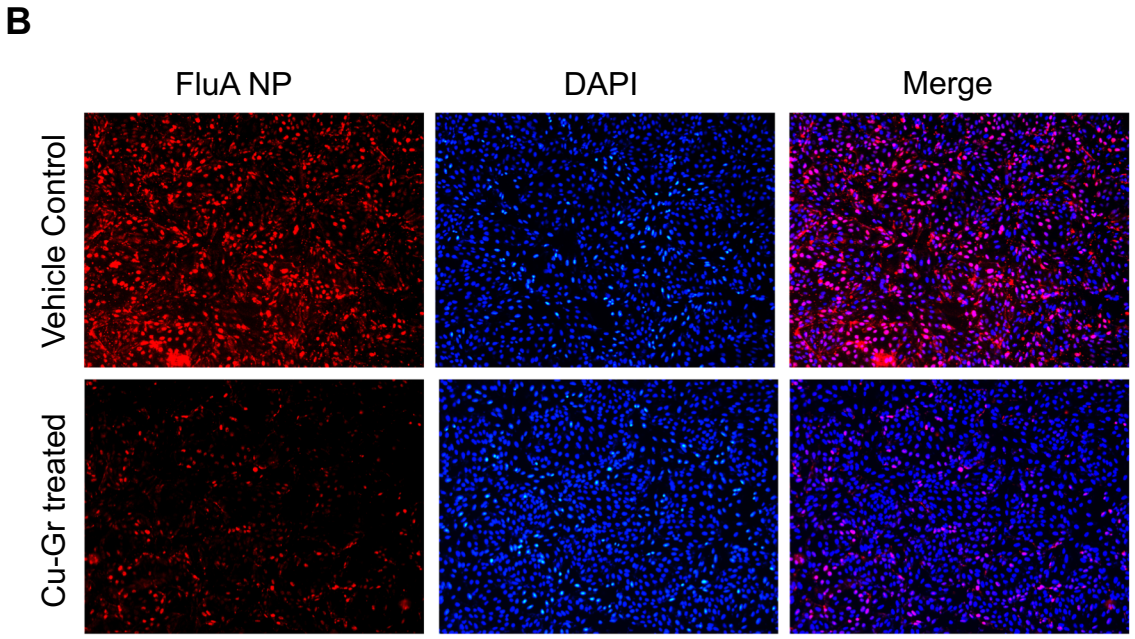
B
FluA NP
DAPI
Merge
Vehicle Control
Cu-Gr treated

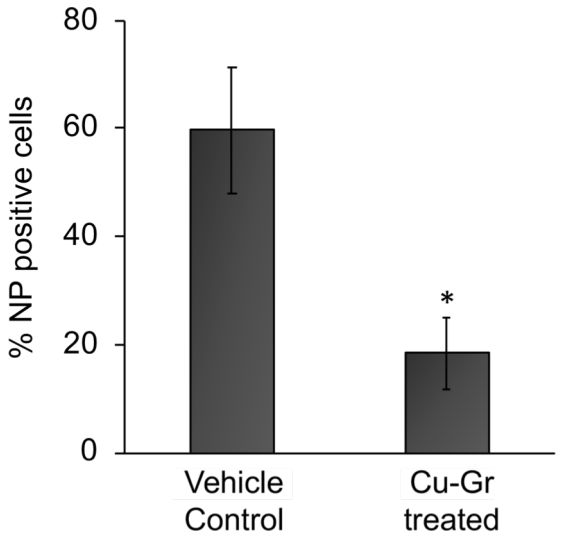
C
% NP positive cells
80
60
40
20
0
*
Vehicle
Control
Cu-Gr
treated

Figure 7

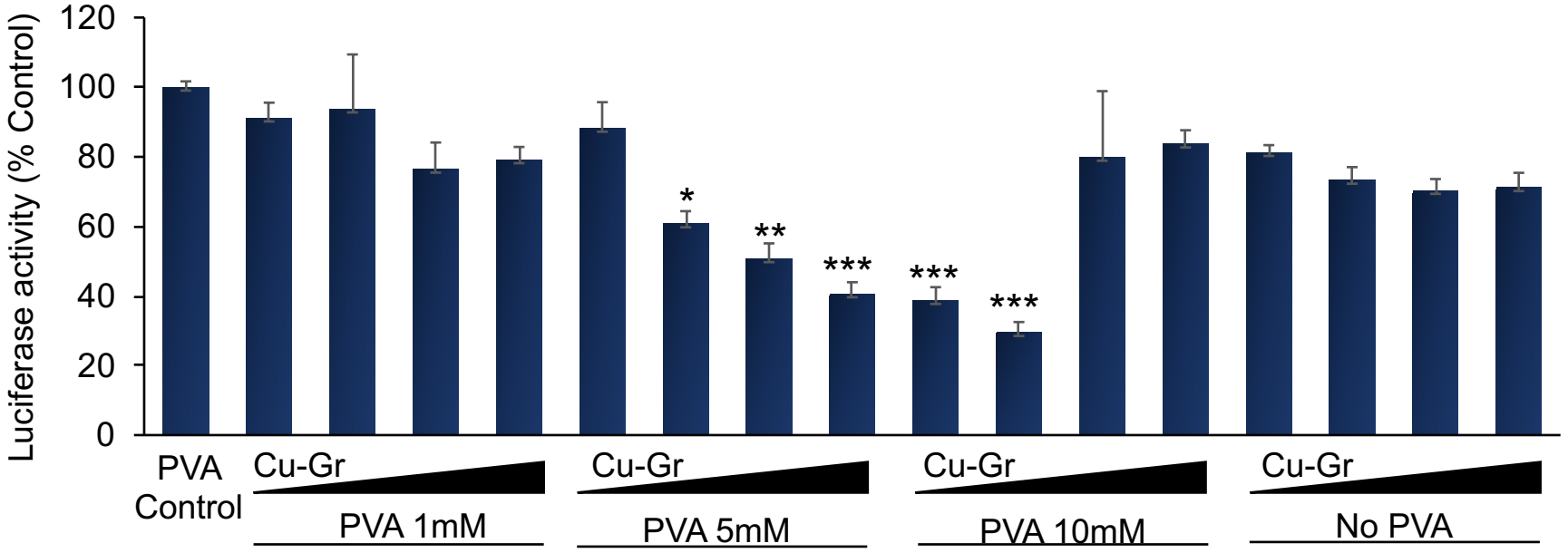
Luciferase activity (% Control)
120
100
80
60
40
20
0
*
**
***
***
***
PVA Control
Cu-Gr
PVA 1mM
Cu-Gr
PVA 5mM
Cu-Gr
PVA 10mM
Cu-Gr
No PVA

Figure 8

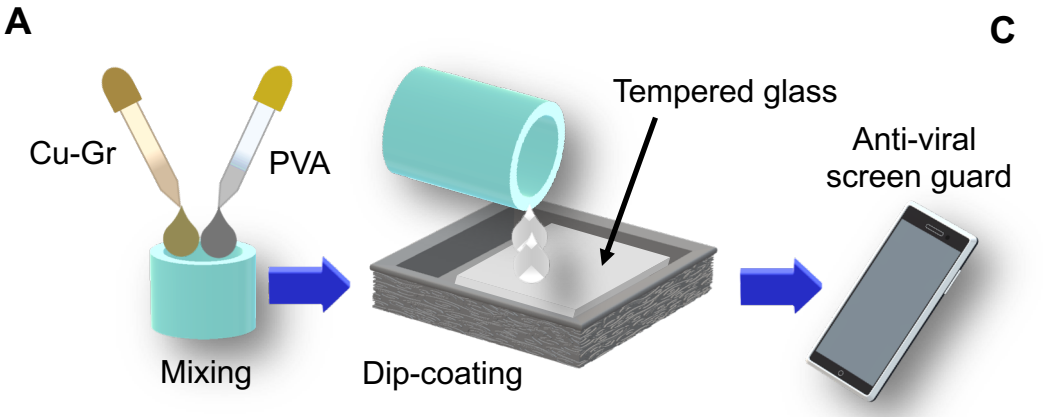
A
Cu-Gr
PVA
Mixing
Tempered glass
Dip-coating
Anti-viral
screen guard


B

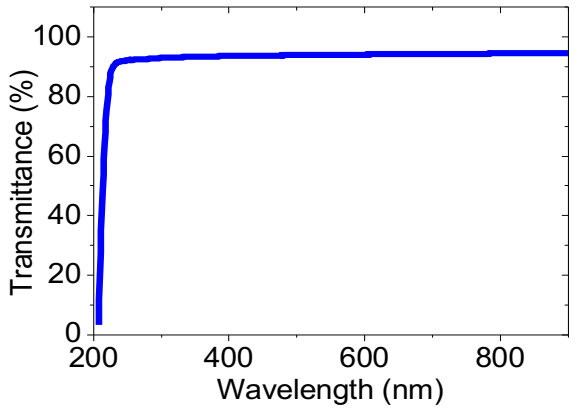
C
Transmittance (%)
100
80
60
40
20
0
200
400
600
800
Wavelength (nm)

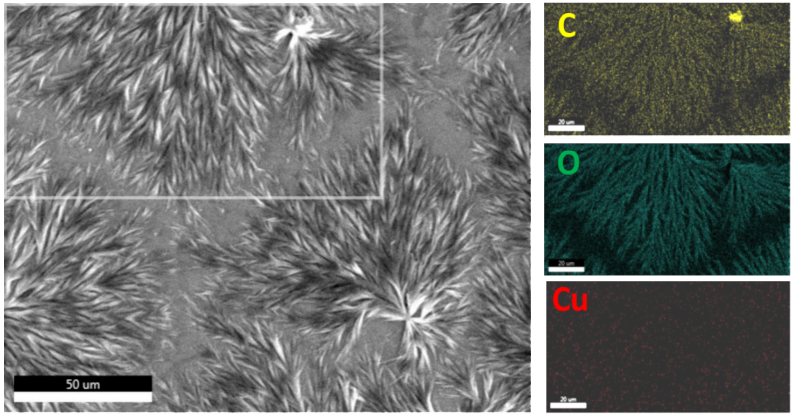
D
50 um
C
O
Cu

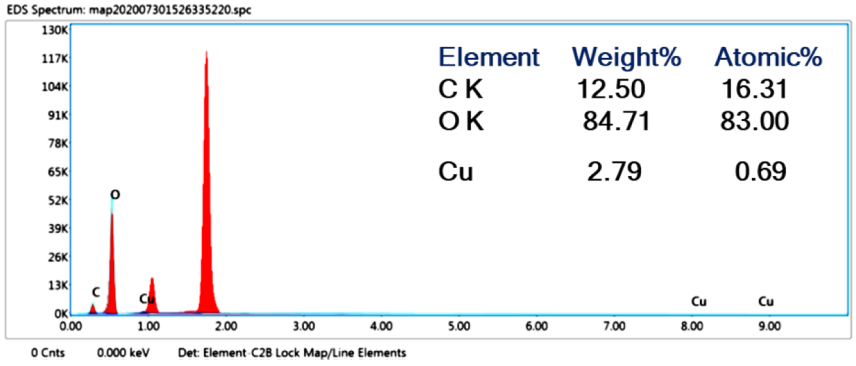
E
EDS Spectrum: map20200730152633522O.spc
Element Weight% Atomic%
C K 12.50 16.31
O K 84.71 83.00
Cu 2.79 0.69
0 Cnts 0.000 keV Det: Element C2B Lock Map/Line Elements

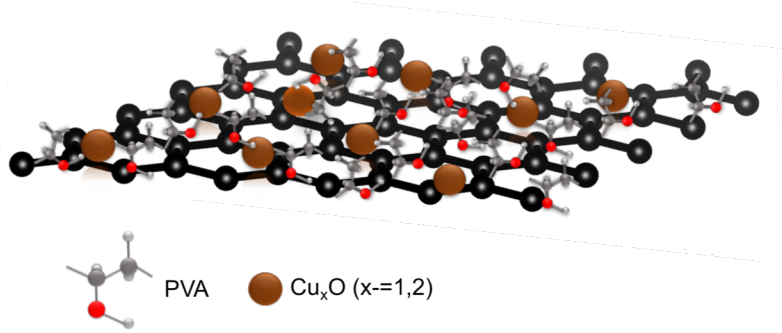
F
PVA
Cu$_x$O (x-=1,2)